encit 2020

ABCM Associação Brasileira de Engenharia e Ciências Mecânicas

18th Brazilian Congress of Thermal Sciences and Engineering
November 16-20, 2020 (Online)

ENC-2020-0651
GRID STUDY FOR ACTIVE FLOW CONTROL APPLIED TO AN AIRFOIL

Bruno Goffert
Instituto Tecnológico de Aeronáutica, Pr Mal Eduardo Gomes, 50, 12228-900, Brazil
bruno.goffert@gmail.com

Ricardo Galdino da Silva
Cayo Prado Fernandes Francisco
Instituto de Aeronáutica e Espaço, Pr Mal Eduardo Gomes, 50, 12224-904, Brazil
ri_galdino@yahoo.com.br, cayo.francisco@gmail.com

Maria Luísa Collucci da Costa Reis
Instituto de Aeronáutica e Espaço, Pr Mal Eduardo Gomes, 50, 12224-904, Brazil
Instituto Tecnológico de Aeronáutica, Pr Mal Eduardo Gomes, 50, 12228-900, Brazil
marialuisamlccr@fab.mil.br

Abstract. *The active flow control applied on the wing surface is an efficient method to prevent or delay flow separations and improve the overall aerodynamic performance. A numerical code based on RANS is used to simulate subsonic flow and steady blowing jet over the airfoil. This paper presents the grid study of an airfoil with different configurations of slat, flap positions and blowing momentum coefficients. The analysis is performed in terms of lift coefficient with the use of the Richardson extrapolation to estimate uncertainties due to mesh refinement and compared to experimental data. Results of drag coefficient are also analyzed according to each grid refinement. Finally, the influence of the proximity of far field to the airfoil is evaluated by the discrepancies of lift coefficient obtained from the simulations.*

Keywords: *Active Flow Control, Steady Blowing Jet, Aerodynamics, CFD, Grid Study.*

1. INTRODUCTION

The improvement of aerodynamic performance using active flow control (AFC) has been remarkable since the middle of the last century. Increase of lift coefficient of three times or more in comparison to the clean configuration and decrease of drag due to delay or suppression of flow separation can be achieved. This is a promising mark regarding the development of STOL (Short Take-off and Landing) aircrafts.

Several types of AFC are used in order to improve aerodynamic performance. Pavlenko et al. (2018) showed results from numerical and experimental analysis of external blown flaps and boundary layer control system for a medium twin-engine STOL aircraft. They utilized the main exhaust turbofan flow on the wings and tangential blowing of compressed air on the high-lift devices, which significantly reduced the fuel consumption, take-off and landing speeds and increased the flight range and payload. Slotnik et al. (2000) used external blown flaps or strakes to investigate the flow in the engine/wing junction. The study showed the reduction of flow separation on the nacelle near the pylon juncture, providing downwash on the upper surface and energizing the boundary layer. Radespiel et al. (2016) conducted extensive studies on steady tangential and oblique blowing jets on the transonic airfoil DLR-F15. The evaluation of tangential blowing was based on the variation of slat configuration, different angles of attack, variations of blowing jet momentum and slot heights. The oblique blowing jet generates longitudinal vortices in the boundary layer, contributing to the increase of turbulent momentum transport and consequently the increase of lift, but some cautions regarding its use are stated. Liu et al. (2004) studied steady blowing jet and pulsed jet employed in the leading edge and trailing edge of the Circulation Control Wing (CCW). The simulations showed good agreement with experimental data in the linear region when the blowing momentum coefficient was varied. Both types of jets increased the lift coefficient, and pulsed jets showed similar gains with lower mass flow rate. Despite the fact that the cited references used different applications on wings and airfoils, the use of Computational Fluid Dynamics (CFD) to simulate their systems is a consensus.

Although the CFD constitutes an effective tool to study the active flow control, we have to take into account several issues to correctly represent the actual flow, such as numerical methods, turbulence models, boundary conditions and the use of appropriate grid. As an initial part of this study, this paper presents the grid analysis for active flow control on an airfoil with slat and flap deployments using tangential steady blowing. First, the grid convergence study is presented by means of lift coefficient values, which are used in the Richardson extrapolation calculation. Then, results are compared to wind tunnel data. Finally, the influence of the proximity of far field to the airfoil is analyzed.

2. METHODOLOGY

This paper is related to the application of the steady tangential blowing jet on the airfoil and high-lift device. The calculation of the bi-dimensional outlet blowing jet, is given by the coefficient below.

$$C_\mu = \frac{m_j V_j}{q_\infty S} = \frac{\rho_j V_j^2 h}{q_\infty c} \tag{1}$$

Where m_j is the blowing mass-flow rate; V_j is the blowing velocity; q_∞ is the free-stream dynamic pressure of the airflow; S is a reference area, ρ_j is the blowing density, h is the slot height and c is the wing chord.

The two dimensional analysis is performed by CFD using a numerical code based on the RANS and Spalart-Allmaras turbulence model. Different angles of attack, blowing velocities and airfoil configurations are considered.

2.1 Richardson Extrapolation

The Richardson extrapolation (RE) has become a widely used method to estimate the uncertainties of the variables resulting from different grid refinement in CFD simulations. An important characteristic of the Richardson extrapolation is that it applies not only to primitive variables, such as velocity or pressure, but also to functions that are the objectives of this study, i.e., the lift coefficient, C_L.

There are three possible convergence types resulting from grid refinement analysis, which are defined below in respect of the ratio of changes R.

Monotonic Convergence: $0 < R < 1$;
Oscillatory Convergence: $R < 0$;
Divergence Convergence: $R > 1$.

Where $R = \varepsilon_{21}/\varepsilon_{32}$. The indexes 1, 2 and 3 are related to the Fine, Medium and Coarse grids, respectively. Then, the difference in solutions between the Coarse and Medium grid is ε_{32}, and between the Medium and Fine grid is ε_{21}.

RE has been an important method to evaluate errors and uncertainties from simulations, but the extrapolation must be used with caution, since the assumption of monotonic convergence is employed. Oscillatory convergence cases are discussed by Celik (2005), which cites recirculation regions near separations and reattachment points and the use of mixed order methods as a source of oscillatory behavior. In the case of divergence convergence, the solutions diverge and errors and uncertainties cannot be estimated (Stern, 1999).

The calculation steps using the Richardson extrapolation are described below, as proposed by the References (ASME, 2009, Celik, 2008, Groves, 2013 and Oberkampf and Trucano, 2002).

Step 1. Calculate the grid parameters for each grid.

$$h = \left[\frac{1}{N}\sum_{i=1}^{N}(\Delta A_i)\right]^{1/2} \tag{2}$$

$$r = h_{coarse}/h_{fine} \tag{3}$$

Where N is the total number of elements, ΔA_i is the area of the ith element and r is the ratio of grid refinement. Celik (2008) and Groves (2013) recommend the use of grid sizes that satisfy $r > 1.3$.

Step 2. Calculate the observed order, p, of the spatial discretization.

$$p = \frac{1}{ln(r_{21})}|ln|\varepsilon_{32}/\varepsilon_{21}| + q(p)| \tag{4}$$

Note that the variable q is a function of the observed order in Eq. (4). Then, we can solve by iterative calculation.

$$q(p) = ln\left(\frac{r_{21}^p - sgn(\varepsilon_{32}/\varepsilon_{21})}{r_{32}^p - sgn(\varepsilon_{32}/\varepsilon_{21})}\right) \tag{5}$$

Step 3. Calculate the extrapolated values, ϕ_{ext}^{21}, and the respective errors, e_a^{21} and e_{ext}^{21}, for the finest and extrapolated grids respectively.

$$\phi_{ext}^{21} = \left(r_{21}^{p}\phi_1 - \phi_2\right)\left(r_{21}^{p} - 1\right) \tag{6}$$

$$e_a^{21} = \left|\frac{\phi_1 - \phi_2}{\phi_1}\right| \tag{7}$$

$$e_{ext}^{21} = \left|\frac{\phi_{ext}^{21} - \phi_1}{\phi_{ext}^{21}}\right| \tag{8}$$

Step 4. Calculate the grid convergence index.

$$GCI_{fine}^{21} = \frac{FSe_a^{21}}{r_{21}^{p} - 1} \tag{9}$$

The *GCI* proposed by Roache (1994), as calculated above (Eq. (9)) for the Fine grid numerical solution, is a method to report grid refinement studies. This converts the discretization error estimate into an uncertainty estimate using absolute values. (Oberkampf and Roy, 2010).

A factor of safety (*FS*) is added to the *GCI* calculation as seen in Eq. (9). Roache (1998) states that the *FS* value should be 1.25 when three grid solutions are used and the observed order of accuracy matches the order of scheme within 10%. Otherwise, a *FS* of 3.0 should be used instead of 1.25 to achieve a 95% certainty over a wide range of applications.

2.2 CFD Code

The SU2 code was used to study the grid refinement for the active flow control on the airfoil. This numerical code is an open source RANS solver capable of simulating the compressible and turbulent flows, which can perform aerodynamic shape optimization (Palacios et al., 2014).

The simulation was based on the Reynolds-Averaged Navier-Stokes equations (RANS), in two-dimensional cases. The Spalart-Allmaras (SA) turbulence model was chosen. The discretization scheme is based on the method of finite volumes in unstructured mesh. Roe's second-order upwind scheme was used to calculate the convective fluxes. Linear system is solved using the iterative FGMRES (Flexible Generalized Minimum Residual) method, and Lower-Upper Symmetric Gauss-Seidel linear preconditioner is used to accelerate the convergence. Since the domain does not present strong non-linearity effects, such as shock waves, and as we are using an implicit method which is not affected by the instability condition when CFL>1, a minimum CFL number of 25 was set for this study.

2.3 Grid

The RAE 102 wing profile with boundary layer control by blowing is studied in this paper. The wing thickness ratio is 0.13. The profile is cambered for a design lift coefficient of 0.2 (Lawford and Foster, 1969). The plain flap is 25% of chord, which is hinged on the lower surface. The blowing jet is applied in the downstream of the slat and in the main body upstream of the flap. The slot allows the jet to be applied tangent to the surface. The nozzle height of the blowing jet is 1.0668×10^{-3} m (0.042 in). The plenum chambers were created in order to supply the required outlet slot condition and simulate the blowing on the airfoil.

The grids were generated by the open source mesh generator Gmsh. The meshes are O-mesh, two-dimensional hybrid type, i.e., formed by quadrilateral and triangular elements. The far field frontier is around 20 chords from the airfoil. All grids have parametric functions that control the number of points and stretching rates on the airfoil and within the domain, ensuring the uniform refinement. Four grids were created for each configuration of slat and flap: Coarse, Medium, Fine and Extra Fine. From the baseline grid and employing a grid refinement factor of two, all other grids were generated identically. Therefore, we doubled and halved the Fine grid, what resulted in the Extra Fine and Medium grid, respectively. Then, we halved the Medium grid to generate the Coarse grid. Once the grid has been refined so that the discretization error is in the asymptotic region, Richardson extrapolation can be used to estimate zero-grid spacing (Iudicelo, 1998).

Table 1 shows the grid configurations with their main characteristics used to evaluate the grid refinement. *N* is the number of total elements, *n* is the number of nodes on the airfoil surface (including plenum chamber) and y^+ is the distance from the wall measured in viscous lengths, which is calculated by a set of equations given by Pope (2000). Figure 1 shows the Coarse grid near the airfoil for 2 different configurations: flap deployed at 20°, and flap deployed at 60° with slat at 30°.

Table 1. Grid characteristics used to the study.

Grid	Slat 0° / Flap 20°			Slat 30° / Flap 60°		
	N	n	y^+	N	n	y^+
Extra Fine, N1	434888	1283	0.09	483390	1477	0.1
Fine, N2	218874	905	1.0	254370	1049	0.9
Medium, N3	107585	635	5.9	127898	734	5.2
Coarse, N4	53976	445	19.7	66757	514	16.2

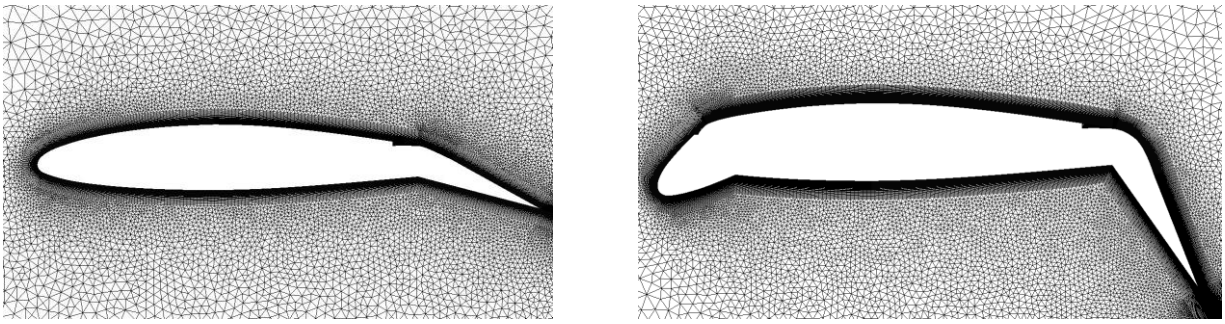

a) Slat 0° and flap 20°. b) Slat 30° and flap 60°.

Figure 1. Coarse grids near the airfoil.

2.4 Configurations and Boundary Conditions

Five cases were chosen to study the grid refinement. Among the cases, there are 2 different configurations: one with flap deployed at 20°, and the other with slat at 30° and flap at 60°. Different settings of tangential blowing jet over the airfoil complete the variations of the cases presented in Tab. 2, where $C\mu_N$ is applied on the leading edge and $C\mu_R$ is applied on the flap. All cases were simulated with airspeed of 44.8 m/s (M = 0.131) and Reynolds number of 3.78×10^6.

Table 2. Case configurations for the grid refinement analysis.

Case	Angle of Attack (AOA)	Slat	Flap	$C\mu_N$	$C\mu_R$
1	10º	0°	20°	0	0
2	10°	0°	20°	0	0.047
3	5º	30°	60°	0	0
4	5º	30°	60°	0	0.060
5	5º	30º	60°	0.025	0.089

The boundary conditions are considered as follows:
- Far field: free stream condition setting velocity as Mach number, angle of attack and temperature;
- Airfoil surface (wall): adiabatic and no-slip condition;
- Inlet nozzle chamber: inlet configuration setting total conditions for pressure and temperature.

In the last condition, temperature is the same as free stream and pressure is adjusted according to the required blowing momentum coefficient at the nozzle exit. This boundary condition is applied only when the blowing is required, otherwise it is considered as wall condition.

3. RESULTS

3.1 Grid Convergence

Figure 2 shows a comparison of pressure coefficient contours and streamlines between the first two cases (Table 2) from Fine grid results. Both airfoils present flaps deployed at 20°, but in Fig.2a) there is no steady blowing applied on the flap and in Fig.2b) steady blowing is applied with $C\mu_R$ = 0.047. Analyzing the streamlines, the suppression of separation behind the flap when the blowing is applied can be clearly noted. In addition, the gain of momentum due to the tangential jet on the flap induces the acceleration of the flow over the main part of the airfoil, which is evidenced by the lower pressure coefficient. Similar results of streamlines and pressure coefficient were found when the blowing is applied to the airfoil with slat deployed at 30° and flap at 60°, as can be seen in Fig. 3.

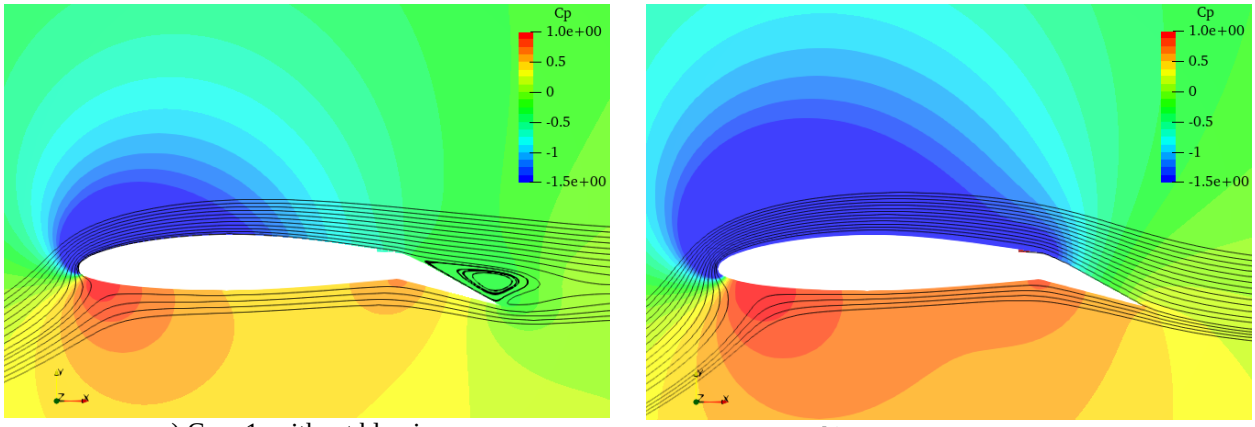

a) Case 1, without blowing. b) Case 2, $C\mu_R$ = 0.047.

Figure 2. Streamlines and pressure coefficient contours over the airfoil with flap deployed at 20°, AOA = 10°.

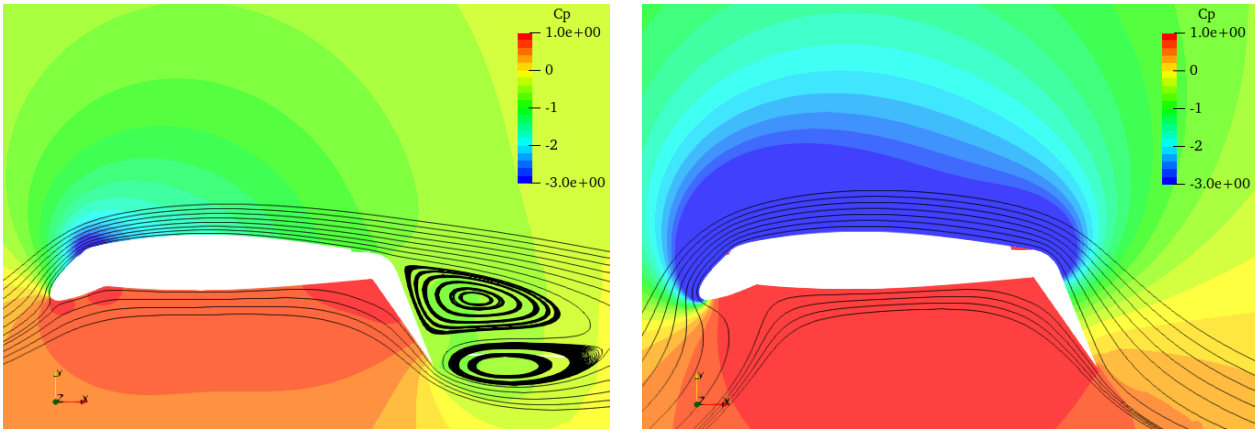

a) Case 3, without blowing. b) Case 5, $C\mu_N$ = 0.025 and $C\mu_R$ = 0.089.

Figure 3. Streamlines and pressure coefficient contours over the airfoil with slat deployed at 30° and flap at 60°, AOA = 5°.

Tables 3 and 4 present the results of the Richardson extrapolation calculation for Cases 1-2 and 3-5, respectively. The method is used in 2 sets of three different grids, N4-N3-N2 and N3-N2-N1, where N1, N2, N3 and N4 are the Extra Fine, Fine, Medium and Coarse grids. They also show the observed order of the numerical method, p, the extrapolated lift coefficient when the grid is converged, Φ_{ext}^{21}, the Fine grid error, e_a^{21}, the uncertainty or grid convergence index of the Fine grid, GCI^{21}, and the deviation compared to the wind tunnel data, $E\Phi_1$. It is possible to see from the tables that the Extra Fine grid can be considered converged and that the Fine grid obtained results close to the converged solutions, but with lower computational costs.

The observed order with the grid set formed by the Coarse, Medium and Fine grid is close to the declared order of 2, and higher orders were found when the Extra Fine grid is considered. The errors (e_a^{21}) and *GCI* were diminished the more the grid was refined. However, in Case 4, where the slat is deployed with the absence of blowing, higher discrepancies and a lack of convergence were observed. The highest numerical error (e_a^{21}) was obtained in this case, notwithstanding the discrepancy of wind tunnel data and the simulation is fairly low, $E\Phi_1$ = 5% with the Fine grid. The error in comparison to experimental data increased more than twice with the Extra Fine grid and the *GCI* increased dramatically to 63.9%. The values can be explained by the small differences between ε_{32} and ε_{21} (R = 0.84), and evidenced by the low observed order which resulted in a high *GCI*. According to Roy (2010), the singularities and discontinuities can impact the ability to obtain reliable estimates of discretization errors, which include issues regarding the presence of shock waves and the sharp leading edge. Figure 4 shows the detail of the step formed by the presence of the slot located between the slat and the main body. The recirculation bubble when the blowing is not applied to the fore slot should be indicative of sources of error, as the flow is attached to the flap with tangential blowing of $C\mu_R$ = 0.060.

In general, the lift coefficient was over predicted in all cases. In the cases of AFC, the flow remains attached to the airfoil surface and the lift coefficient presented a better agreement with the wind tunnel experiment.

Table 3. Richardson extrapolation calculation for the airfoil with flap deployed at 20°. Cases 1 and 2 of Table 2.

Configuration	Case 1, $C\mu = 0$		Case 2, $C\mu_R = 0.047$	
Φ_{exp}	$C_L = 1.632$		$C_L = 2.794$	
Grids	N4, N3, N2	N3, N2, N1	N4, N3, N2	N3, N2, N1
Φ_1	1.858	1.859	2.953	2.947
Φ_2	1.771	1.858	2.849	2.953
Φ_3	1.634	1.771	2.568	2.849
p	1.385	13.733	2.944	8.101
Φ_{ext}^{21}	1.995	1.859	3.009	2.947
$\boldsymbol{e_a^{21}}$	**4.7%**	**0.04%**	**3.5%**	**0.20%**
$\boldsymbol{GCI^{21}}$	**9.2%**	**0.0004%**	**2.4%**	**0.02%**
$\boldsymbol{E\Phi_1}$	**13.9%**	**14.0%**	**5.7%**	**5.5%**

Table 4. Richardson extrapolation calculation for the airfoil with slat deployed at 30° and flap at 60°. Cases 3 to 5 of Table 2.

Configuration	Case 3, $C\mu = 0$		Case 4, $C\mu_R = 0.060$		Case 5, $C\mu_N = 0.025$ and $C\mu_R = 0.089$	
Φ_{exp}	$C_L = 1.813$		$C_L = 4.187$		$C_L = 5.145$	
Grids	N4, N3, N2	N3, N2, N1	N4, N3, N2	N3, N2, N1	N4, N3, N2	N3, N2, N1
Φ_1	2.148	2.155	4.394	4.663	5.552	5.604
Φ_2	2.105	2.148	4.073	4.394	5.280	5.552
Φ_3	2.008	2.105	3.561	4.073	4.867	5.280
p	2.626	5.229	1.564	0.333	1.412	4.731
Φ_{ext}^{21}	2.177	2.156	4.846	7.047	5.988	5.619
$\boldsymbol{e_a^{21}}$	**2.0%**	**0.3%**	**7.3%**	**5.8%**	**4.9%**	**0.9%**
$\boldsymbol{GCI^{21}}$	**1.7%**	**0.1%**	**12.8%**	**63.9%**	**9.8%**	**0.3%**
$\boldsymbol{E\Phi_1}$	**18.5%**	**18.8%**	**5.0%**	**11.4%**	**7.9%**	**8.9%**

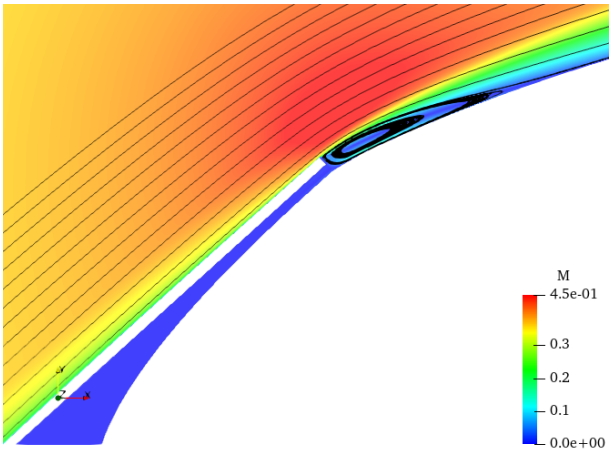

Figure 4. Recirculation on the slat for Case 4.

Figures 5 and 6 plot the convergence curves of the lift and drag coefficients. The abscissa refers to 1/N, which is the proportional element spacing and the ordinates are C_L and C_D. In all cases the lift coefficient tends towards the convergence, except in case 4. The drag coefficients also show that the convergence is close for Cases 1, 2, 3 and 5, where deviations between Fine and Extra Fine grids are low. The curve C_D for Case 4 did not show any change of trend with N1, N2 and N3 grids. Thus, more grids are necessary to obtain values related to converged solution.

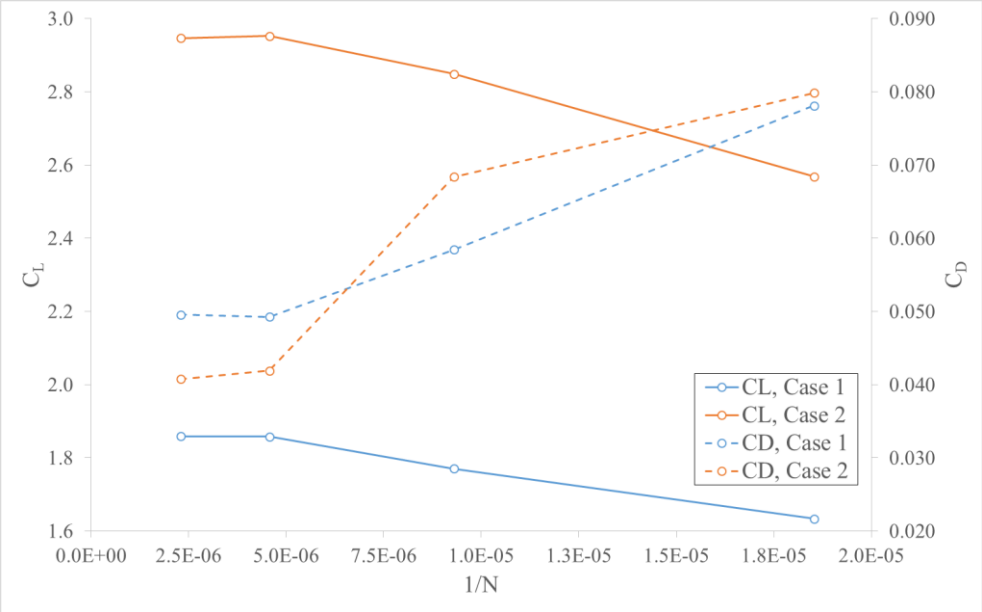

Figure 5. Grid convergence of the lift and drag coefficients, slat 0° and flap 20°.

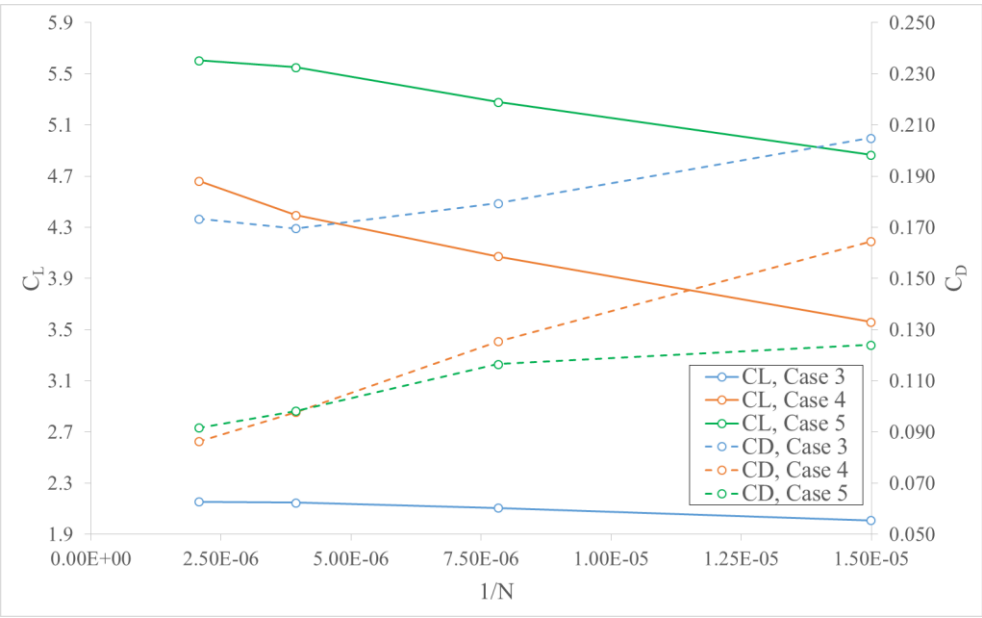

Figure 6. Grid convergence of the lift and drag coefficients, slat 30° and flap 60°.

Figure 7 presents a summary of results in terms of lift coefficient with the error bars calculated by Eq. (9) for the Fine and Extra Fine grids. The error bar for case 4 with Extra Fine grid was not considered due to the non-asymptotic solution. The relative errors between Fine and Extra Fine grid are also showed in the plot, since Cases 1, 2, 3 and 5 using Extra Fine grids converged. Although the solutions in Cases 1 and 5 present high values in the error bars, with *GCI* of 9.2% and 9.8% respectively, the discrepancies of lift coefficients between the Fine and Extra Fine grid are not significant, with relative errors lower than 1%. For this reason, we believe that the Fine grid is suitable for AFC studies on the airfoil. Note that the error bars for cases 1, 2, 3 and 5 with the Extra Fine grids are not visible in the plot, with *GCI* of 0.3% in the worst case, which suggests that the solutions converged. Comparing the relative errors with the estimated uncertainties for the Fine grid due to the grid discretization, the Richardson extrapolation method seems overestimate the uncertainties, which would allow the reduction of the factor of safety (*FS*) to one in Eq. (9).

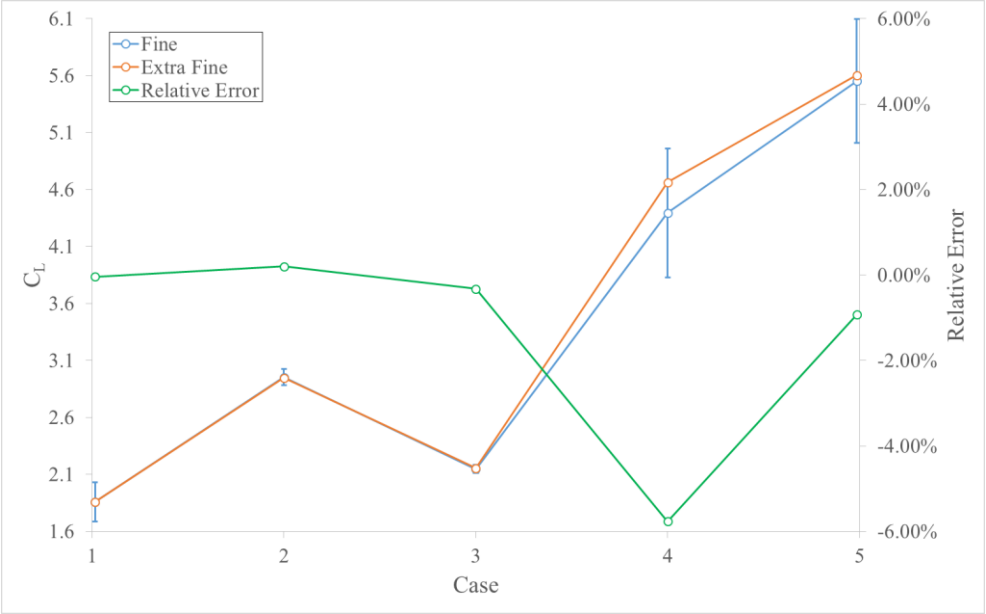

Figure 7. Lift coefficient solutions with error bars and relative errors.

3.2 Influence of far field

Due to high deviations found when the slat and flap are deployed, an investigation based on the influence of the proximity of the far field to the airfoil was performed. New meshes were generated with the far field 100 chords distant from the airfoil. The core of the mesh was kept the same as the Fine grid, N2 (see Table 1), and a ring domain surrounding the baseline grid was added. The grid generation scheme is shown below in Fig. 8 (a).

Figure 8 (b) shows the differences of lift coefficient between the baseline and the extended far field. According to Fig. 8 (b), similar values were found in each case. The analysis did not show correspondence with the increasing of lift coefficient or application of the blowing on the airfoil, and the differences seem random with gains and losses of C_L. The maximum deviation presented is 0.017 (0.39%) for Case 4, which is the case of slat deployed at 30º and flap at 60° with blowing jet momentum of 0.060 on the flap. Discrepancies below 0.004 were obtained in Cases 1, 3 and 5, and 0.011 in the Case 2. Therefore, the far field distant 20 chords to the airfoil used in the baseline grid does not significantly affect the results.

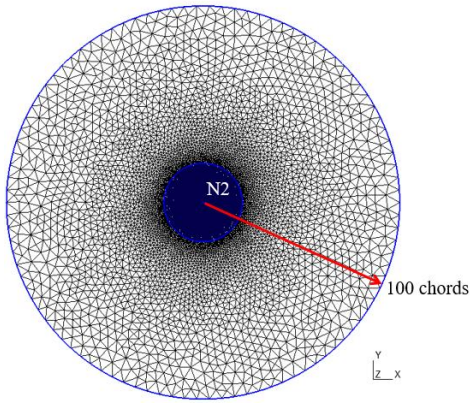

a) Grid scheme with far field distant 100 chords from the airfoil.

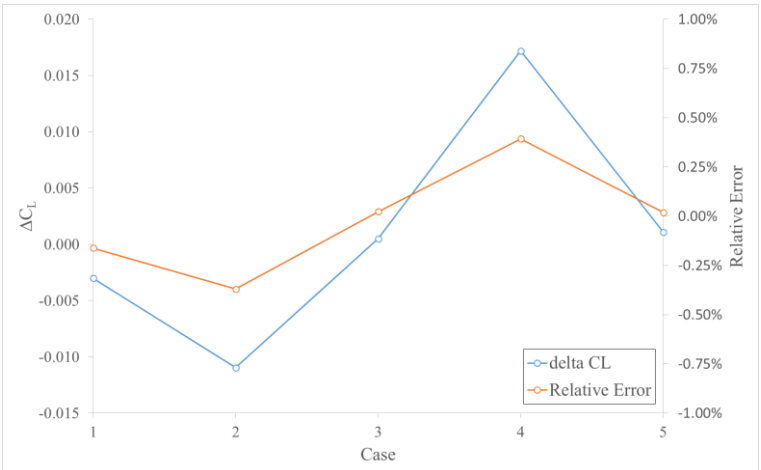

b) Deviation and relative error of lift coefficient between the baseline grids and extended far field.

Figure 8. Study of influence of far field to the lift coefficient.

4. CONCLUSIONS

The grid study for active flow control on the RAE 102 airfoil has been performed using simulations based on the RANS with Spalart-Allmaras turbulence model. Four grids were generated for the study and the solutions were used to estimate the uncertainties due to grid refinement by Richardson extrapolation method and compared to experimental data. From the results it is possible to conclude that the Extra Fine grid presented the converged solutions, and the Fine grid can be used for other studies with reduced computational costs. The Richardson extrapolation showed its potential to estimate the uncertainties, but analyzing the differences of the lift coefficient between the Fine and Extra Fine grids, the uncertainties seem to be overestimated when the Fine grid solution is considered. The case of the deployed slat without blowing did not present an asymptotic solution, which renders the uncertainties useless for the Extra Fine grid. A possible cause could be the recirculation bubble formed in the step between the deflected slat and the main body. In general, the results in terms of lift coefficient were overestimated and they were closer to experimental data when the blowing was used. In these cases the flow separation was suppressed and the lift coefficient was increased. In the latter, the proximity of the far field to the airfoil was evaluated due to the deviations of lift coefficient in comparison to experimental data. Solutions from two different far field locations were compared and no evidence of the influence of the far field over the airfoil was observed. Thus, the far field located at 20 chords from the airfoil is adequate for this study.

5. ACKNOWLEDGEMENTS

This study was financed in part by the Coordenação de Aperfeiçoamento de Pessoal de Nível Superior – Brasil (CAPES) – Finance Code 88887.465118/2019-00. The authors would like to express their gratitude to the São Paulo Research Foundation for the support of this study through grant FAPESP/CEPID 2013/07375-0.

6. REFERENCES

ASME, 2009. Standard for Verification and Validation in Computational Fluid Dynamics and Heat Transfer, *The American Society of Mechanical Engineers*, ASME V&V 20-2009.

Celik, I., Li, J., Hu, G., Shaffer, C., 2005. Limitations of Richardson extrapolation and some possible remedies, *Journal of Fluids Engineering*, 127, pp. 795-805.

Celik, I. B., Ghia, U., Roache, P. J., Freitas, C. J, 2008. Procedure for estimating and reporting of uncertainty due to discretization in CFD applications, *American Society of Mechanical Engineers Journal of Fluids Engineering*, Vol. 130.

Groves, C. E, LLie, M., Shallhorn P. A., 2013. Comprehensive approach to verification and validation of CFD simulations applied to backward facing step-application of CFD uncertainty analysis, In *Proceeding of the 51st AIAA Aerospace Sciences Meeting including the New Horizons Forum and Aerospace Exposition*, AIAA 2013-0258, Dallas/Ft. Worth TX, United States.

Iudicello, F., 1998. Guide for the verification and validation of computational fluid dynamics simulations, AIAA G-077-1998.

Liu, Y., Sankar, L. N., Englar, R. J., Ahuja, K. K., Gaeta, R., 2004. Computational evaluation of the steady and pulsed jet effects on the performance of a Circulation Control Wing section, In *Proceedings of the 42nd AIAA Aerospace Sciences Meeting and Exhibit*, AIAA2004-56, Reno NE, United States.

Lawford, J. A., Foster, D. N., 1969. Low-speed wind tunnel tests on a wing section with plain leading- and trailing-edge flaps having boundary-layer control by blowing, Reports and Memoranda No. 3639 (London Her Majesty's Stationery Office).

Oberkampf, W. L. and Trucano, T. G., 2002. Verification and validation in Computational Fluid Dynamics, Technical Report SAND2002-0529, Unlimited Release.

Oberkampf, W. L. and Roy, C. J., 2010. *Verification and validation in scientific computing*, Cambridge University Press.

Palacios, F., Economon, T. D., Aranake, A., Copeland, S. R., Lonkar, A. K, Lukaczyk, T. W., Manosalvas, D. E., Naik, K. R., Padron, S., Tracey, B., Variyar, A., Alonso, J. J., 2014. Stanford University Unstructured (SU2): Analysis and Design Technology for Turbulent Flows, In *Proceedings of the 52nd Aerospace Sciences Meeting, American Institute of Aeronautics and Astronautics*, AIAA2014-0243, National Harbor, MD, United States.

Pavlenko, O., Petrov, A., Pigusov, E., 2018. Concept of medium twin-engine STOL transport airplane, In *Proceedings of the 31st Congress of the International Council of the Aeronautical Sciences*, Belo Horizonte, Brazil.

Pope, S. B., 2000. *Turbulent Flows*, Cambridge University Press, pp. 269-270.

Radespiel, R., Burnazzi, M., Casper, M., Scholz P., 2016. Active flow control for high lift with steady blowing, *The Aeronautical Journal*, Vol. 120, No. 1223, pp. 171-200.

Roache, P. J., 1994. Perspective - A method for a uniform reporting of grid refinement studies, *Journal of Fluids Engineering*, Vol. 116:3, pp. 405-411.

Roache, P. J., 1998. *Verification and Validation in Computational Science and Engineering*, Albuquerque, NM, Hermosa Publishers.

Roy, C. J., 2010. Review of discretization error estimators in scientific computing, In *Proceedings of the 48th AIAA Aerospace Sciences Meeting Including the New Horizons Forum and Aerospace Exposition*, AIAA2010-126, Orlando FL, United States.

Slotnick, J.P., An, M. Y., Mysko, S. J., Yeh, D. T., Rogers, S. E., Roth, K., Baker, M. D., Nash, S. M., 2000. Navier-Stokes analysis of a high wing transport high-lift configuration with externally blown flaps, In *Proceedings of the 18th AIAA Applied Aerodynamics Conference*, AIAA2000-4219, Denver CO, United States.

Stern, F., Wilson, R. V., Coleman, H. W., Paterson, E. G., 1999. Verification and validation of CFD simulations, Iowa Institute of Hydraulic Research, IIHR Report No. 407.

7. RESPONSIBILITY NOTICE

The authors are the only responsible for the printed material included in this paper.